

Forecasting Cosmic Parameter Errors from Microwave Background Anisotropy Experiments

J.R. Bond¹, G. Efstathiou² and M. Tegmark^{3,4}

¹ CIAR Cosmology Program, CITA, University of Toronto, Toronto, ON M5S 3H8, Canada; bond@cita.utoronto.ca

² Department of Physics, University of Oxford, g.efstathiou1@physics.oxford.ac.uk

³ Institute for Advanced Study, Princeton, NJ 08540, USA; max@ias.edu

⁴ Hubble Fellow

arXiv:astro-ph/9702100v1 12 Feb 1997

ABSTRACT

Accurate measurements of the cosmic microwave background (CMB) anisotropies with an angular resolution of a few arcminutes can be used to determine fundamental cosmological parameters such as the Hubble constant H_0 , the density parameter Ω_0 and the baryon density parameter Ω_b , to a precision of about a percent or better. Assuming the true theory is a variant of inflationary cold dark matter cosmologies, we calculate the accuracy with which cosmological parameters can be determined by the next generation of CMB satellites, MAP and Planck. We pay special attention to: (a) the accuracy of the computed derivatives of the CMB power spectrum C_ℓ ; (b) the number and choices of parameters; (c) the inclusion of prior knowledge of the values of various parameters.

Key words: cosmology: theory — cosmic background radiation

1 INTRODUCTION

The detection of primordial anisotropies in the microwave background radiation by the COBE satellite (Smoot et al. 1992) has had an enormous impact on cosmology (see White, Scott and Silk 1994 and Bond 1996 for reviews). However, the relatively poor angular resolution of COBE/DMR ($\theta_{fwhm} \approx 7^\circ$) limits the amount of information that can be extracted from the CMB. From the 4 year COBE maps (Bennett et al. 1996), the overall amplitude of the CMB power spectrum for a given spectral shape has been determined to an accuracy of 7% and a power law index characterizing the shape to about 25%.^{*} Constraints on other parameters such as Ω_0 and on the cosmological constant Λ are weak.

It has long been known (e.g. Sunyaev and Zeldovich 1970) that at angular resolutions smaller than $\sim 1^\circ \Omega_0^{1/2}$ (the angle subtended by the Hubble radius at the time of recombination) the CMB power spectrum will depend on e.g., the sound speed of the baryon-photon fluid, and hence on a number of fundamental cosmological parameters, such as the net cosmological density parameter Ω_0 , the Hubble

constant H_0 and the baryon density Ω_b . In adiabatic models, the acoustic motions of the matter-radiation fluid lead to a characteristic series of ‘Doppler peaks’ in the CMB power spectrum which have been investigated in considerable detail numerically and semi-analytically (e.g., Bond 1996, Hu et al. 1997). Similar behaviour is expected qualitatively in defect (isocurvature) theories, though the pattern of Doppler peaks is expected to be less distinct and has not yet been calculated to high precision (e.g., Turok 1996). We therefore restrict the discussion in this paper to purely adiabatic perturbations obeying Gaussian statistics, as expected in most inflationary models of the early universe (e.g., Linde 1990). The anisotropies in such models can be computed to high accuracy which, as we will show in Section 2, is essential for estimating the precision with which cosmological parameters can be determined from the CMB.

Intermediate angle experiments have detected temperature anisotropies which are consistent with a primordial origin and in rough agreement with adiabatic theory predictions. However, the accuracy and robustness of the results does not yet allow strong conclusions to be drawn, even when experimental results are combined together (e.g., Bond 1996, Bond & Jaffe 1996, Lineweaver et al. 1997, Rocha & Hancock 1997). An experiment with an angular resolution of $\theta_{fwhm} \sim 5'$ can yield useful information about the CMB spectrum C_ℓ up to multipoles beyond a Gaussian filtering scale $\ell_s = \sqrt{8 \ln 2} \theta_{fwhm}^{-1} \sim 2000$, and each multipole is statistically independent (assuming complete sky coverage). However, it is clear from visual inspection (e.g.

^{*} $\langle \ell(\ell+1)C_\ell/(2\pi) \rangle_{dmr}^{1/2} = 1.03 \pm 0.07 \times 10^{-5}$ for the best-fit primordial index, which is $n_s = 1.02 \pm 0.24$ (e.g., Bond 1996). The temperature power spectrum is defined as the expectation value $C_\ell = \langle |a_{\ell m}|^2 \rangle$, where the coefficients $a_{\ell m}$ are defined by a spherical harmonic expansion of the temperature anisotropies on the celestial sphere $\Delta T/T = \sum_{\ell m} a_{\ell m} Y_{\ell m}(\theta, \phi)$.

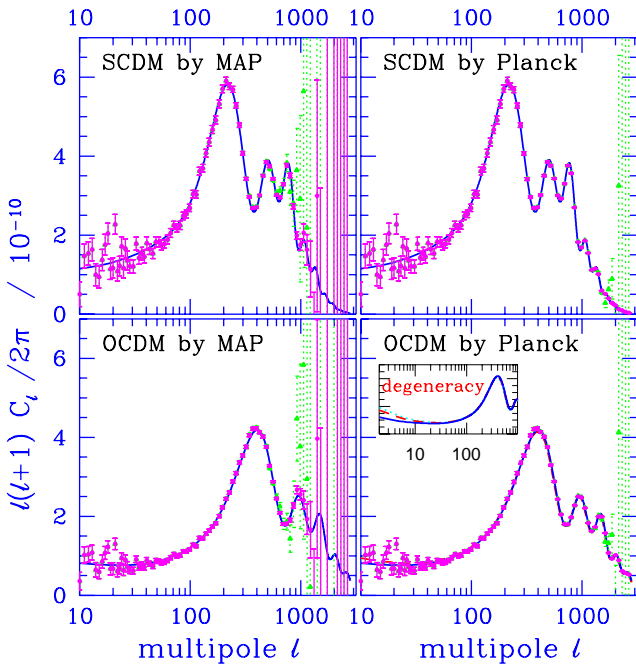


Figure 1. Temperature power spectra for a standard CDM (SCDM) model with $h = 0.5$ and $\Omega_0 = 1$ and an open CDM (OCDM) model with $h = 0.6$ and $\Omega_0 = 0.33$. The points show a quadratic power spectrum estimation of C_ℓ (in bands of width 5% in ℓ), along with the one sigma error, from simulated CMB skies observed by the MAP and Planck satellites described in Section 3 and Table 1. The solid errors in the left panels use the MAP⁺ parameters for the three highest frequency channels and two years of observing, while the dotted errors give the original MAP specifications with one year of observing. The solid errors in the right panel use the four lowest frequency Planck HFI channels, and follow the theoretical curves precisely far down the damping tail for OCDM and SCDM models, while the dotted errors show the three highest frequency LFI channels for Planck. In the bottom right panel, a C_ℓ curve with $\Omega_0 = 0.59$, $\Omega_{vac} = 0.44$ and $h = 0.9$ almost degenerate with the OCDM model is superposed. The inset, showing these two and also a $\Omega_0 = 0.68$, $\Omega_{vac} = 0.58$ and $h = 1.1$ model, demonstrate that the angle-distance degeneracy surface (see text) used to define these models is almost exact; these models can be distinguished only at low multipoles no matter how precise the CMB experiment.

Figure 1) that a typical inflationary C_ℓ curve is smooth and can be specified accurately by many fewer than 2000 parameters. It is therefore not obvious *a priori* to what extent the typically 10-15 parameters specifying an inflationary model can be disentangled by a particular set of measurements. Evidently, a detailed calculation is necessary as has been performed in an important paper by Jungman et al. (1996). However, as described in the next section, an accurate assessment of the degeneracies between cosmological parameters imposed by high resolution CMB experiments requires a precise numerical calculation, rather than the semi-analytic approach adopted by Jungman et al.

2 PARAMETER ESTIMATION WITH PRIORS

2.1 The covariance matrix

Errors on a set of cosmological parameters \mathbf{s} are estimated using Bayes theorem, which updates the prior probability $P(\mathbf{s}|\text{prior})$ for the parameters with a likelihood function $\mathcal{L}(\mathbf{s})$: $P(\mathbf{s}) \propto \mathcal{L}(\mathbf{s})P(\mathbf{s}|\text{prior})$. (Although a uniform prior seems to be the least prejudicial, there are certain non-debatable restrictions and plausible constraints which are reasonable to include as prior information, as discussed in Section 2.5.) If the errors $\delta\mathbf{s} \equiv \mathbf{s} - \mathbf{s}_0$ about the mean $\mathbf{s}_0 = \langle \mathbf{s} \rangle$ are small, then an expansion of $\ln \mathcal{L}$ to quadratic order about the maximum gives:[†]

$$\mathcal{L} \approx \mathcal{L}_m \exp \left[-\frac{1}{2} \sum_{ij} F_{ij} \delta s_i \delta s_j \right],$$

$$F_{ij} = \sum_\ell (\Delta C_\ell)^{-2} \frac{\partial C_\ell}{\partial s_i} \frac{\partial C_\ell}{\partial s_j}, \quad (1)$$

$$(\Delta C_\ell)^2 \approx \frac{2}{(2\ell+1)f_{\text{sky}}} \left(C_\ell + \overline{w}^{-1} \overline{\mathcal{B}}_\ell^{-2} \right)^2, \quad (2)$$

$$\overline{w} \equiv \sum_c w_c, \quad \overline{\mathcal{B}}_\ell^2 \equiv \sum_c \mathcal{B}_{c\ell}^2 w_c / \overline{w}, \quad (3)$$

$$w_c \equiv (\sigma_{c,\text{pix}} \theta_{c,\text{pix}})^{-2}, \quad \mathcal{B}_{c\ell}^2 \approx e^{-\ell(\ell+1)/\ell_s^2},$$

adopting a Gaussian approximation for the beam function $\mathcal{B}_{c\ell}$. In this approximation, with a uniform prior the covariance matrix $\mathbf{M} \equiv \langle \delta\mathbf{s}\delta\mathbf{s}^\dagger \rangle$ is the inverse of Fisher information matrix \mathbf{F} (e.g., Tegmark et al. 1997), the 1-sigma error on s_i is $\sigma_i = M_{ii}^{1/2}$, the numbers quoted in Table 2, and the correlation coefficient between parameters i and j is $r_{ij} = M_{ij}/(\sigma_i \sigma_j)$. Equation (2) gives the standard error ΔC_ℓ on the estimate of C_ℓ to an experiment with N frequency channels c for an experiment with angular resolution $\theta_{c,fwhm}$ and sensitivity $\sigma_{c,\text{pix}}$ per resolution element ($\theta_{c,fwhm} \times \theta_{c,fwhm}$ pixel), sampling a fraction f_{sky} of the sky.

A key simplifying assumption in deriving equation (2) is that the noise is homogeneous and isotropic. Although this will never be true in practice, and determining how to handle the inhomogeneity for large datasets will be a challenge for the future, accurate error estimates can be obtained using the average weight for the smooth inhomogeneity expected. Equation (2) is exact if $f_{\text{sky}} = 1$ (e.g., Knox 1995) and is approximately correct at multipoles $\ell \gtrsim \ell_{\text{cut}}$ corresponding to angular scales small compared to the dimensions $2\pi/\ell_{\text{cut}}$ of an incomplete sky map. The accuracy of cosmological parameter estimation via the covariance matrix approach therefore depends on: (1) the validity of the Gaussian approximation to the likelihood function; (2) the number and choice of the parameters \mathbf{s} defining the theoretical model; (3) the parameters \mathbf{s}_0 of the target model; (4) the numerical accuracy of the derivatives of C_ℓ ; (5) the inclusion of

[†] The likelihood also has terms which depend upon the deviations of the specific realization of the theory represented by the observations from the ensemble-averaged values used here (Bond 1996). We have tested these effects in detail on parameter estimation and find them to be small and fully consistent with the error estimates we quote in the Tables.

prior constraints on the parameters \mathbf{s} ; (6) systematic errors in estimates of C_ℓ caused by Galactic and extragalactic foregrounds. For high resolution experiments which tightly constrain many of the cosmological parameters, a Gaussian approximation about the maximum likelihood should be quite good (Knox 1995, Spergel private communication), although positivity and other constraints can truncate general excursions in the likelihood space. We ignore systematic errors caused by foreground subtraction, since over much of the sky these are very likely to be much smaller than the variance of equation (2) (see *e.g.* Tegmark and Efstathiou 1996, for a discussion of foreground removal from CMB maps). Here we consider the remaining four points.

2.2 Choice of variables

Parameters describing the theoretical angular power spectra include those for initial conditions and those characterizing the transport of radiation through photon decoupling to the present. If we were to allow all possible variations, the count of parameters could easily exceed 20; in our analysis, we use ≤ 11 variables. Initial conditions could be very complicated; here we characterize them by an overall amplitude and a spectral index (tilt) for the scalar and tensor components, $\mathcal{P}_\Phi^{1/2}(k_n)$ and n_s , $\mathcal{P}_{GW}^{1/2}(k_n)$ and n_t . The primordial amplitude parameters for the gravitational potential fluctuations, $\mathcal{P}_\Phi^{1/2}(k_n)$, and the gravity wave fluctuations, $\mathcal{P}_{GW}^{1/2}(k_n)$, are chosen here to be normalized at a wavenumber corresponding to the horizon scale. Possible complications, which we ignore here, include the variations of the spectral indices with wavenumber k (parameterized in Jungman et al. by a running term, $dn_s/d\ln k$), isocurvature as well as adiabatic components in the scalar perturbations, and non-Gaussian fluctuations.

At the time of decoupling, the key parameters determining the temperature power spectrum are the densities of various types of matter, the expansion rate, the sound speed, and the damping rate; all of these depend only on the density parameters $\omega_j \equiv \Omega_j h^2$, where $j = b, cdm, hdm, \gamma, erv$ refers to baryons, cold dark matter, hot dark matter, and the various relativistic particles present then, such as photons and relativistic neutrinos. The Hubble parameter[†] at that time only depends upon $\omega_{nr} = \omega_b + \omega_{cdm} + \omega_{hdm}$ (if the massive neutrinos were nonrelativistic then) and $\omega_\gamma = \omega_\gamma + \omega_{erv}$. Massive neutrinos become nonrelativistic below a redshift $\sim 1700(m_\nu/\text{ev})^{-1}$, where $\omega_{hdm} \approx 0.01(m_\nu/\text{ev})N_{\nu}$, N_{ν} is the number of neutrino species of mass m_ν ; for small m_ν , the neutrinos may be relativistic or semirelativistic at decoupling.

The transport to an angular structure of scale ℓ^{-1} now from the post-decoupling spatial pattern of temperature fluctuations of comoving scale k^{-1} depends on the cosmological angle-distance relation, $\ell \sim k\mathcal{R}$, where

$$\frac{\omega_{nr}^{1/2}\mathcal{R}}{3000 \text{ Mpc}} = \frac{\omega_{nr}^{1/2}}{\omega_k^{1/2}} \sinh \left[\int \frac{\omega_k^{1/2} da}{(\omega_k + \omega_{vac}a^2 + \omega_{nr}a^{-1})^{1/2}} \right]$$

for an open universe (*e.g.*, Bond & Efstathiou 1984). Here

[†] h is the present value of the Hubble parameter H_0 in units of $100 \text{ km s}^{-1}\text{Mpc}^{-1}$; it is related to the ω_j by $h^2 = \sum_j \omega_j$.

$\omega_{vac} \equiv \Omega_{vac}h^2$ parameterizes the energy density associated with a cosmological constant Λ ($\Omega_{vac} = \Lambda/(3H_0^2)$) and $\omega_k \equiv (1 - \Omega_0)h^2$ parameterizes the energy associated with the mean curvature of the universe. This results in a degeneracy along $\delta(\omega_{nr}^{1/2}\mathcal{R}) = 0$ lines, which leads to a linear relation between $\delta\omega_k$ and $\delta\omega_{vac}$ for fixed ω_{nr} , with coefficients that depend upon the explicit target model. The angular pattern we observe also depends upon the change of the gravitational metric in time between post-decoupling and the present, which breaks this degeneracy. However, this late-time integrated Sachs-Wolfe effect influences only low multipoles which have a large cosmic variance. Thus, there exists one combination of variables which cannot be determined accurately from CMB observations alone, even with a high precision experiment such as the Planck Surveyor, as the lower right panel of Fig. 1 illustrates.

Some parameters are well constrained by measurements other than CMB anisotropies. For example, ω_γ depends on the temperature T_0 of the CMB, ω_{erv} depends as well on the number of massless neutrino types N_{erv} ; the C_ℓ 's also depend on the relative amount of hydrogen and helium, parameterized by Y_{He} . Rather than allow them complete freedom, we use the prior probability to restrict their allowed variations. (Since the experimental errors on Y_{He} , T_0 and N_ν are small[§], they have a small effect on other cosmological parameters and hence we only use Y_{He} in our analysis here to illustrate these effects.)

There also could be many parameters needed to characterize the ionization history of the Universe; here we just use the Compton optical depth τ_C from a reheating redshift z_{reh} to the present, assuming full ionization. We therefore analyse a maximum of 11 parameters in this paper: Y_{He} , τ_C , 4 initial condition parameters and 5 density parameters ω_j .

For a given model, the amplitudes of the scalar and tensor power spectra are uniquely related to the observed amplitude of the CMB power spectrum and that of the present day mass fluctuations (characterised, for example, by the *rms* density fluctuation in spheres of radius $8 h^{-1} \text{ Mpc}$, σ_8). For example, Jungman et al. used the quadrupole $C_2^{1/2}$ to fix the amplitude of the fluctuation spectrum. We usually use $\langle \ell(\ell+1)C_\ell/(2\pi) \rangle_B^{1/2}$, an average over the total band B of multipoles that is accessible to the experiment, since this is most accurately determined. However σ_8 and $\mathcal{P}_\Phi^{1/2}(k_n)$ are of sufficient physical interest that we also show the accuracies with which these can be determined. To characterize the tensor amplitude, we use $r_{ts} \equiv C_2^{(T)}/C_2^{(S)}$. In inflation models, there is a relation between $\mathcal{P}_{GW}^{1/2}(k_n)/\mathcal{P}_\Phi^{1/2}(k_n)$ and the tensor tilt, with small corrections dependent upon the scalar and tensor tilts, which can make one of the variables redundant for this class of models. Similarly r_{ts} would be a function of the tilts and other cosmological parameters (*e.g.*, Bond 1996).

Although any parameter set which defines a coordinate system on the likelihood surface is a viable set, parameters for which the Fisher matrix analysis is particularly well suited are those for which the first order expansion $C_\ell = C_\ell(\mathbf{s}_0) + (\partial C_\ell(\mathbf{s}_0)/\partial \mathbf{s}) \cdot (\mathbf{s} - \mathbf{s}_0)$ is more accurate than

[§] $Y_{He} = 0.23 \pm 0.01$ (Pagel et al. 1992), $T_0 = 2.728 \pm 0.004$ (Fixsen et al. 1997), $N_\nu = 2.991 \pm 0.016$ (LEP Electroweak Working Group 1995).

the sampling variance ΔC_ℓ of equation 2 over a few standard deviations of \mathbf{s} from the target set \mathbf{s}_0 . The set of variables that we have adopted gives acceptably high accuracy for the CMB experiments described in Section 3.

2.3 Choice of target models

We analyze a spatially flat ($\Omega_0 = 1$) target model and one with mean curvature. For the canonical flat one we use a standard CDM model (SCDM) with the following parameters: $n_s = 1$, $n_t = 0$, $\Omega_0 = 1.0$, $\Omega_b = 0.05$, $r_{ts} = 0$, $\Omega_{cdm} = 0.95$, $\Omega_{hdm} = 0$, $h = 0.5$, $\tau_C = 0$, $Y_{He} = 0.23$. The target model is normalized to match COBE DMR, which has $\sigma_8 = 1.2$. The open model has $h = 0.6$, $\Omega_0 = 0.33$, $\Omega_b = 0.035$, $\Omega_{cdm} = 0.30$ and $\sigma_8 = 1$. For the open model, the role of gravity waves on large angular scales is still under debate so we ignore the tensor component in that case. (All models have a 13 Gyr cosmological age.) The SCDM does not agree with large scale observations, so we discuss results for two other DMR-normalized flat models: a spatially flat $h = 0.5$ HCDM model with 2 species of massive neutrinos, with $\Omega_{hdm} = 0.2$, $m_\nu = 2.4$ eV, $\sigma_8 = 0.77$, and an $h = 0.7$ Λ CDM model with $\Omega_\Lambda = 0.67$, $\sigma_8 = 1.1$.

2.4 Accuracy of the power spectrum derivatives

Computational errors in the derivatives of C_ℓ can lead to large errors in the covariance matrix. We distinguish between two classes of error, one caused by inadequate semi-analytic approximations to the C_ℓ and the second caused by numerical errors in C_ℓ and its derivatives computed from linear Boltzmann transport codes. The C_ℓ accuracy must be 1% or better, especially for high resolution experiments probing multipoles $\ell \gtrsim 1000$ where the expected random errors on each individual multipole become $\lesssim 3\%$. Errors which are weakly correlated with physical parameters are particularly serious since these can artificially break real near-degeneracies between cosmological parameters, and lead to overly optimistic estimates by an order of magnitude or more. Extreme care is therefore required in computing the C_ℓ derivatives. For this work we have used derivatives calculated with two Boltzmann transport codes, an updated version of the multipole code described by Bond and Efstathiou (1987) generalized to low density universes and including tensor components (Bond 1996 and references therein), and the fast path-history code developed recently by Seljak and Zaldarriaga (1996). Generally the C_ℓ 's from these codes agree to better than 1%. We use intervals of typically 1–5% in the parameters \mathbf{s} in computing numerical derivatives of C_ℓ , *i.e.* small enough that the derivatives are insensitive to the size of the interval, but large enough that they are unaffected by numerical errors in the C_ℓ coefficients. The primary limitation on the error estimates for Table 2 should be the C_ℓ linearization assumption made in deriving equation 1, although we believe that better than percent level accuracy in C_ℓ is needed to achieve high precision in the nearly degenerate directions of parameter space. The differences between our error estimates and analogous results of Jungman et al. , which are large for some parameters, are caused primarily by their use of semi-analytic approximations to calculate C_ℓ and its derivatives.

2.5 Inclusion of prior information on parameters

We have mentioned that a non-uniform $P(\mathbf{s}|\text{prior})$ is particularly useful for parameters such as Y_{He} and T_0 , where other experiments restrict their values to much higher accuracy than can be achieved from CMB experiments alone. For other parameters, *e.g.* h and ω_b , it may be that the distribution derived from a CMB experiment is much narrower than any reasonable prior distribution, in which case we gain little by including prior information. There are also intermediate cases where prior information can help break degeneracies between parameters estimated from the CMB alone. We approximate the prior distribution of parameter values by a Gaussian distribution with covariance matrix \mathbf{T} , so the covariance matrix of parameter values including prior information is given by

$$\mathbf{M} = (\mathbf{F} + \mathbf{T}^{-1})^{-1} \text{ if } P(\mathbf{s}|\text{prior}) \propto e^{-\frac{1}{2}\delta\mathbf{s}^t \mathbf{M}^{-1} \delta\mathbf{s}} \quad (4)$$

(*e.g.* Knox 1996), where \mathbf{F} is the Fisher matrix (1). If we are interested in the error bars on s_i irrespective of the values of the other variables, we would marginalize over these, with error $\sigma_i = M_{ii}^{1/2}$ for the Gaussian case. For most of the entries in Table 2 we use no prior at all ('noP'), except for Y_{He} where indicated. When priors are used, we adopted the following values: 0.3 on the normalization $\delta\langle C_\ell \rangle_B^{1/2} / \langle C_\ell \rangle_B^{1/2}$, 0.5 on n_s , 2 on r_{ts} , 0.075 on ω_b , 1 on ω_{nr} , 1 on ω_{vac} , 1 on ω_k , 0.5 on ω_{mv} , and 1 on τ_C . There are some variables that are restricted, *e.g.*, to be positive, which can also be incorporated into the prior, but at the expense of more complicated expressions after marginalization over these constrained variables. In some cases, this leads to a factor of two or more improvement in the accuracy of some parameters.

Generally the errors in the parameters will be correlated through nondiagonal components of $(\mathbf{F} + \mathbf{T}^{-1})^{-1}$. Linear combinations of the parameters which are uncorrelated can be found by diagonalizing $(\mathbf{F} + \mathbf{T}^{-1})$. When the eigenvalues of $(\mathbf{F} + \mathbf{T}^{-1})$ are rank ordered, from highest to lowest, the variable combinations corresponding to high values will be very accurately determined, while those for the lowest may be very poorly determined, representing the most degenerate directions in parameter space. In Tables 2 and 3 below we list the number of parameter combinations that are determined within a ± 0.01 and ± 0.1 accuracy.

3 COSMOLOGICAL PARAMETER ERRORS FROM MAP AND PLANCK

3.1 The CMB power spectrum estimated from MAP and Planck

In this section we apply the above machinery to determine the accuracy of cosmological parameter estimation from two satellite experiments: the MAP satellite selected by NASA (Bennett et al. 1996) and the Planck Surveyor Mission (formerly named COBRAS/SAMBA) selected by ESA (Bersanelli et al. 1996). These satellites offer examples of the best that is likely to be achieved in the next decade. Ground based and balloon borne experiments will certainly continue to provide improved constraints on cosmological parameters over this timescale, and so we also analyze a sample long duration balloon experiment (LDB).

The specifications adopted for MAP and Planck are

listed in Table 1 and have been computed from the information provided on the respective WWW pages for the two missions. Although indicative of the expected performance of each satellite at the time of writing, these are likely to evolve. Of the 5 HEMT channels for MAP, we assume that the 3 highest frequency channels, at 40, 60 and 90 GHz, will be dominated by the primary cosmological signal. We also present the gains that result from a 25% improvement in angular resolution at all frequencies and 2 years of observing time (we denote these specifications by MAP⁺). Planck will have two detector arrays, a Low Frequency Instrument (LFI) using HEMTs and a High Frequency Instrument (HFI) using bolometers. The current design of the HFI incorporates an additional channel at 90GHz in addition to channels at 150, 217 and 353GHz; we have adopted parameters as listed in Table 2 for these four channels. We also present results for the 3 highest resolution channels in the current design of the Planck LFI which has an expected performance that is significantly improved over those given by Bersanelli et al. (1996).

For each ℓ , the computational procedure automatically rotates the channels into a linear combination optimal for the CMB. However, a more sophisticated treatment is needed to remove Galactic and extragalactic foregrounds. We ignore this complication here and assume instead that the CMB power spectrum can be determined over $f_{sky} = 0.65$, in which Galactic foregrounds are negligible. This is similar to the ‘clean’ sky area adopted in most analyses of the COBE power spectrum.

Figure 1 shows examples of C_ℓ estimates from one realization of the SCDM and OCDM target models. In this figure, the estimated power spectra have been averaged over 5% wide bands in ℓ . At the resolution of MAP there is very little useful information beyond the third doppler peak ($\ell \lesssim 800$), whereas Planck samples the power-spectrum at close to the theoretical variance limit to multipoles $\ell \sim 2000$. The consequences of these differences for CMB parameter estimation are described in the next section.

3.2 Accuracy of cosmological parameters

Results of the analysis for the sample LDB experiment and for the MAP and Planck satellites are given in Table 2. For the LDB example we take specifications for TopHat, which would cover 4.3% of the sky with an error of $18\mu\text{K}$ per $20'$ pixel (which includes an allowance for the extra error incurred in removing foregrounds). We assume 65% of this area will be usable. Because the sky coverage is so limited, COBE’s DMR is added to improve the baseline in ℓ covered and thus the accuracy of parameter estimation. (When we apply our analysis to DMR alone, using the average noise in the 53+90+31 GHz map, $\bar{\sigma}_{pix} \approx 30\mu\text{K}$ per $5.2'$ pixel, we predict the bandpower would be determined to 0.07 and n_s to 0.20 for SCDM, 0.07 and 0.28 for OCDM, if only these two parameters are used, in agreement with what is actually found (Section 1); with all 9 parameters, the errors grow, but the first and second eigenparameter combinations have error estimates of 0.09 and 0.20 for SCDM. When treating two experiments at very different scales, such as DMR and the long duration balloon experiment example shown, the log likelihoods (and Fisher matrices) just add.

For each target model, we list the errors $\sigma_i = M_{ii}^{1/2}$ on the parameters derived with and without a prior distribution for MAP. Even for MAP the prior results have little impact, provided variables such as Y_{He} are constrained. If the helium abundance is allowed to freely float, it has a substantial effect on the parameters; controlling its variation to be 0.23 ± 0.02 has little impact on the other numbers, so we could take the 9 parameters in the SCDM part of Table 2 as 10. The prior distributions make negligible difference to the results for Planck and hence we present only the no-prior results in Table 2.

As expected, some of the parameters, such as the power amplitude $\langle C_\ell \rangle_B^{1/2}$ and τ_C , and ω_k , ω_{vac} and ω_{nr} (and ω_{hdm}) are highly correlated in all models; e.g., the correlation coefficients between these parameter pairs are about 90% for SCDM for Planck and MAP with similar results holding for the other models. Thus, although our estimates of errors after marginalization are gratifyingly small for many parameters, especially for the specifications of Planck, they are large in other cases (e.g. $\delta\Omega_{vac}h^2$). Error estimates in square brackets are those obtained when the most correlated component for that variable is constrained to be the target value; for the power amplitudes, this is τ_C ; for ω_{vac} it is ω_k . A more natural way to deal with strong correlations between variables is to perform a principle component analysis in parameter space, rank-ordering linear linear combinations of parameters, as described in Section 2.5: some linear combinations are determined exquisitely well and some are less well determined because of near-degeneracies as is illustrated in the Tables. The Tables also show values obtained in round brackets when positivity constraints on parameters such as τ_C are used.

The $\delta h/h$ shown are determined from $h^2 = \sum_j \omega_j$, hence it is a derived rather than fundamental quantity. However, h errors depend upon what is kept fixed and what is varied. Thus we can use h to replace one of ω_{nr} , ω_{vac} , ω_k , with the other two to be marginalized. In that case, the error estimate would be $\delta h/h = 0.5\delta\omega_j/h^2$.

We find that the estimated errors on parameters are sensitive to their input target-model values. Table 3 shows results for two other $\Omega_0 = 1$ models, a ΛCDM model and an HCDM model. This illustrates the sensitivity of parameter error estimation to relatively modest changes in the target C_ℓ . In interpreting these tables it is also important to take into account the restrictions that we have imposed on the models: the HCDM model is assumed to be spatially flat, hence Ω_{curv} is constrained to be zero in this case; in the OCDM model we have constrained the amplitude of the tensor component to be zero.

We have also found that the errors on n_t and r_{ts} are extremely dependent on the input r_{ts} if they are allowed to vary independently (Knox and Turner 1994, Knox 1995, Efstathiou 1997). However, h and the various matter densities, ω_{cdm} etc., are insensitive to the tensor spectrum for reasonable values of $r_{ts} \lesssim 2$. In open universes, features in the power-spectrum shift to larger multipoles according to the angle-distance relation, roughly as $C(\ell) \rightarrow C(\ell/\Omega_0^{1/2})$; thus, for low Ω_0 , high resolution is required to determine parameters which affect the Doppler peak structure (e.g. h and the various ω). The relative accuracies of the parameters are less sensitive to variations of Ω_b and h .

4 CONCLUSIONS

In summary, we have described how to compute the errors in the estimation of cosmological parameters from measurements of the CMB power spectrum at a number of frequencies with different angular resolutions and sensitivities. We have also shown how prior information on the values of parameters can be incorporated into the analysis and described some of the pitfalls of this type of analysis that can arise if inaccurate derivatives of the C_ℓ 's are used and if poor parameter choices are adopted.

We have applied our machinery to the MAP and Planck satellites and find that these missions are capable of determining fundamental cosmological parameters to an accuracy that far exceeds that from conventional astronomical techniques. In particular, Planck is capable of determining the Hubble constant and the baryon density parameter Ω_b to a precision of a few percent or better for each of the target models listed in Tables 2 and 3. However, some parameter combinations are poorly determined by CMB observations alone as described in Section 2.3 and Section 3. Nevertheless, despite this caveat, it is evident from this work that accurate CMB observations have the potential to revolutionize our knowledge of the key cosmological parameters describing our Universe.

We would like to thank Lloyd Knox for useful discussions. JRB was supported by the Canadian Institute for Advanced Research and NSERC. GPE acknowledges the award of a PPARC Senior Research Fellowship. MT was supported by NASA through a Hubble Fellowship, #HF-01084.01-96A, awarded by the Space Telescope Science Institute, which is operated by AURA, Inc. under NASA contract NAS5-26555.

REFERENCES

Bennett C. et al. 1996; MAP home page, <http://map.gsfc.nasa.gov>

Bersanelli, M. et al. 1996, COBRAS/SAMBA, The Phase A Study for an ESA M3 Mission, ESA Report D/SCI(96)3; Planck home page, <http://astro.estec.esa.nl/SA-general/Projects/Cobras/cobras.html>

Bennett, C. et al. 1996 Ap. J. Lett., **464**, 1.

Bond J.R. & Efstathiou G., 1984, ApJ Lett., **285**, L45.

Bond J.R. & Efstathiou G., 1987, MNRAS, **226**, 665.

Bond, J.R. 1996, *Theory and Observations of the Cosmic Background Radiation*, in "Cosmology and Large Scale Structure", Les Houches Session LX, August 1993, ed. R. Schaeffer, Elsevier Science Press, and references therein.

Bond, J.R. & Jaffe, A. 1997, in Proc. XXXI Rencontre de Moriond, ed. F. Bouchet, Edition Frontières, in press; astro-ph/9610091.

Efstathiou G. 1997, in Proc. XXXI Rencontre de Moriond, ed. F. Bouchet, Edition Frontières, in press.

Fixsen, D.J. et al. 1996, Ap. J., in press.

Hu, W., Sugiyama, N. & Silk, J. 1997, astro-ph/9504057, Nature, in press.

Jungman G., Kamionkowski M., Kosowsky A. & Spergel D.N. 1996 Phys. Rev. D**54**, 1332.

Knox, L. & Turner, M. S. 1994, Phys. Rev. Lett., **73**, 3347.

Knox L., 1995, Phys. Rev. D**48**, 3502.

Kogut, A. et al. 1996, ApJ, **464**, L29.

LEP Electroweak Working Group 1995, CERN preprint PPE/95-172.

Lineweaver, C. et al. 1997, preprint astro-ph/9610133.

Linde A. 1990, *Particle Physics and Inflationary Cosmology*, Harwood Academic Publishers.

Netterfield, C.B., Devlin, M.J., Jarosik, N., Page, L. & Wollack, E.J. 1997, ApJ, **474**, 47.

Pagel B.E.J., Simonson E.A., Terlevich R.J. & Edmunds M.G., 1992, MNRAS, **255**, 325.

Rocha, G. & Hancock, S. 1997, preprint astro-ph/9611228.

Seljak U. & Zaldarriaga M. 1996, ApJ, **469**, 437.

Smoot G.F. et al., 1992, ApJ, **396**, L1.

Sunyaev R.A. & Zeldovich Ya. B., 1970, Ap&SS, **7**, 3.

Tegmark M. & Efstathiou G., 1996, MNRAS, **281**, 1297.

Tegmark, M., Taylor, A. & Heavens, A. F. 1997, astro-ph/9603021, ApJ, in press.

Turok N., 1996, ApJ Lett., **473**, L5.

White, M., Scott, D. & Silk, J. 1994, Ann. Rev. Astron. Ap. **32**, 319.

Table 1. Experimental Parameters adopted for this study. ν_{ch} denotes the central frequency of the channel, θ_{fwhm} the resolution, σ_{pix} the pixel sensitivity (in $\Delta T/T$) per θ_{fwhm}^2 resolution element, ℓ_s is the Gaussian beam filter scale, and w^{-1} is the noise power for each channel.

MAP (first 3 used)					
ν_{ch} (GHz)	90	60	40	(30)	(22)
θ_{fwhm}	18'	23'	32'	(39')	(54')
$\sigma_{pix}/10^{-6}$	13	9.9	7.3	(6)	(4)
$w^{-1}/10^{-15}$	4.5	4.5	4.5		
ℓ_s	465	345	255		
MAP ⁺ ($w^{-1} \times 0.5$ (2 yrs), $\theta_{fwhm} \times 0.75$)					
$w^{-1}/10^{-15}$	2.3	2.3	2.3		
ℓ_s	620	460	340		
Planck HFI (first 4 used)					
ν_{ch} (GHz)	90	150	220	350	(545) (857)
θ_{fwhm}	16'	10'	6.6'	4.1'	(4.4') (4.4')
$\sigma_{pix}/10^{-6}$	1.1	1.3	1.2	16	(77) (4166)
$w^{-1}/10^{-15}$	0.028	0.015	0.005	0.35	
ℓ_s	505	800	1225	1970	
Planck LFI (first 3 used)					
ν_{ch} (GHz)	100	65	44	(30)	
θ_{fwhm}	10'	14'	21'	(30')	
$\sigma_{pix}/10^{-6}$	2.0	3.7	3.7	(5.5)	
$w^{-1}/10^{-15}$	0.31	0.50	0.22		
ℓ_s	810	580	385		

Table 2. Parameter estimation for the 2 models shown. The standard CDM model has $\Omega_0 = 1$, $h = 0.5$. The open CDM model has $\Omega_{tot} = 0.33$, $h = 0.6$. The columns refer to experimental parameters for a fiducial Long Duration Balloon Experiment (LDB), and MAP and Planck, with parameters listed in Table 1. MAP⁺ assumes a 25% improvement in beams and 2 years as opposed to 1 year of observing. **P** means the prior constraint controls that parameter's value. Values in square brackets indicate results on that variable when its dominate correlation is removed. Results in circular brackets indicate what happens when a positivity constraint is imposed. Results for these cases are only given for significant variations. In the satellite cases, $\ell_{cut} = 2$ was chosen, but for the LDB experiment $\ell_{cut} = 12$ was used. Figures in brackets give error estimates that include positivity constraints. The LDB parameters are based upon ten day's observing with the bolometer-based TopHat experiment with 65% of a 24° radius patch being usable. HEMT-based LDBs (e.g., UCSB's BEAST) could in principle achieve similar accuracy levels. Because of the limited sky coverage the LDB likelihood is combined with the DMR likelihood to constrain low ℓ 's. DMR has $\bar{w}^{-1}/10^{-15} = 950$.

Param	LDB P	MAP no P	MAP P	MAP ⁺ no P	Planck(LFI) no P	Planck(HFI) no P
$\bar{w}^{-1}/10^{-15}$	1.5	1.5	1.5	.77	0.17	.0033
f_{sky}	.028	.65	.65	.65	.65	.65
SCDM MODEL						
Orthogonal Parameter Combinations within ε						
$\varepsilon < 0.01$	1/9	2/9	2/9	3/9	3/9	5/9
$\varepsilon < 0.1$	4/9	6/9	6/9	6/9	6/9	7/9
Single Parameter Errors from Marginalizing Others						
$\delta \langle \mathcal{C}_\ell \rangle_B^{1/2} / \langle \mathcal{C}_\ell \rangle_B^{1/2}$.022	.019 (.012)	.019 (.012)	.017	.019	.016 [.008]
δn_s	.19	.06 (.03)	.06 (.03)	.04	.01	.006
δr_{ts}	.86	.38 (.30)	.34	.25	.12	.09
$\delta \Omega_b h^2 / \Omega_b h^2$.20	.09 (.06)	.08 (.06)	.05	.016	.007
$\delta \Omega_{nr} h^2 / h_0^2$.39	.18 (.11)	.16 (.10)	.11 (.07)	.04 (.02)	.02 [.012] (.006)
$\delta \Omega_{vac} h^2 / h_0^2$.87	.43 (.38)	.47	.40	.19	.12 [.05]
$\delta \Omega_{curv} h^2 / h_0^2$.15	.05	.04	.027	.010	.005 [.002]
$\delta \Omega_{\nu\mu} (h)^2 / h_0^2$.25 P	.08	.07	.05	.04	.03 [.014]
τ_C	.30	.22	.21	.19	.18	.16
$\delta Y_{He} / Y_{He}$.09 P	.09 P (1.4)	.09 P	.09 P (.59)	.08 P (.19)	.07 P (.10)
$\delta h/h$.43	.20	.18	.15	.08	.05 [.02]
$\delta \sigma_8 / \sigma_8$.28	.29	.20	.20	.21	.17 [.09]
$\delta \mathcal{P}_\Phi^{1/2}(k_n) / \mathcal{P}_\Phi^{1/2}(k_n)$.24	.24	.18	.20	.17	.15 [.02]
OPEN CDM MODEL						
Orthogonal Parameter Combinations within ε						
$\varepsilon < 0.01$	2/7	2/7	2/7	2/7	3/7	5/7
$\varepsilon < 0.1$	4/7	4/7	5/7	5/7	6/7	7/7
Single Parameter Errors from Marginalizing Others						
$\delta \langle \mathcal{C}_\ell \rangle_B^{1/2} / \langle \mathcal{C}_\ell \rangle_B^{1/2}$.03	.02 [.016]	.02	.02	.02	.017 [.004]
δn_s	.13	.04	.04	.02	.01	.003
$\delta \Omega_b h^2 / \Omega_b h^2$	1.3	.32	.32	.13	.03	.01
$\delta \Omega_{nr} h^2 / h_0^2$.64	.17	.17	.10	.05	.02 [.005]
$\delta \Omega_{vac} h^2 / h_0^2$	1.5	.46	.45	.33	.18	.07
$\delta \Omega_{curv} h^2 / h_0^2$.23	.06	.06	.03	.007	.002
τ_C	.26	.12	.12	.11	.07	.06
$\delta h/h$.76	.23	.22	.17	.09	.04
$\delta \sigma_8 / \sigma_8$.29	.43 [.26]	.25	.26	.12	.07 [.02]
$\delta \mathcal{P}_\Phi^{1/2}(k_n) / \mathcal{P}_\Phi^{1/2}(k_n)$.30	.64 [.49]	.27	.31	.19	.07 [.02]

Table 3. Parameter estimation for the untilted Λ CDM model, with $\Omega_{vac} = 0.66$, $\Omega_{tot} = 1$, $h = 0.70$, and the untilted HCDM model, with $h = 0.50$ and 2 species of neutrinos with the same mass giving $\Omega_{m\nu} = 0.2$, $\Omega_{tot} = 1$. The columns are as in Table 3.

Param	LDB P	MAP no P	MAP P	MAP+ no P	COSA(LFI) no P	COSA(HFI) no P
$\bar{w}^{-1}/10^{-15}$	1.5	1.5	1.5	.77	0.17	.0033
f_{sky}	.028	.65	.65	.65	.65	.65
Λ CDM MODEL						
Orthogonal Parameter Combinations within ε						
$\varepsilon < 0.01$	1/9	2/9	2/9	3/9	4/9	5/9
$\varepsilon < 0.1$	4/9	6/9	6/9	6/9	7/9	7/9
Single Parameter Errors from Marginalizing Others						
$\delta \langle \mathcal{C}_\ell \rangle_B^{1/2} / \langle \mathcal{C}_\ell \rangle_B^{1/2}$.021	.019	.019 (.010)	.018	.020	.017 [.007]
δn_s	.20	.07 (.04)	.06 (.04)	.05	.017	.010
δr_{ts}	.85	.27 (.20)	.26 (.20)	.20	.10	.08
$\delta \Omega_b h^2 / \Omega_b h^2$.36	.10	.09	.06	.02	.008
$\delta \Omega_{nr} h^2 / h_0^2$.36	.12	.12	.08	.03	.02 [.01]
$\delta \Omega_{vac} h^2 / h_0^2$	1.3	.43 (.32)	.41 (.32)	.34	.17	.10 [.03]
$\delta \Omega_{curv} h^2 / h_0^2$.07	.02 (.014)	.017 (.014)	.01	.004	.002 [.0006]
$\delta \Omega_{m\nu} (h)^2 / h_0^2$.17	.04	.04	.03	.02	.014
τ_C	.29	.19	.18	.18	.17	.15
$\delta h/h$.54	.17	.16	.14	.07	.042
$\delta \sigma_8 / \sigma_8$.29	.29	.21	.24	.20	.16 [.08]
$\delta \mathcal{P}_\Phi^{1/2}(k_n) / \mathcal{P}_\Phi^{1/2}(k_n)$.28	.38	.23	.27	.19	.14 [.02]
HCDM MODEL						
Orthogonal Parameter Combinations within ε						
$\varepsilon < 0.01$	0/8	1/8	2/8	2/8	3/8	4/8
$\varepsilon < 0.1$	3/8	5/8	5/8	5/8	6/8	6/8
Single Parameter Errors from Marginalizing Others						
$\delta \langle \mathcal{C}_\ell \rangle_B^{1/2} / \langle \mathcal{C}_\ell \rangle_B^{1/2}$.021	.017 (.014)	.017	.016	.018	.013 [.008]
δn_s	.14	.10 (.05)	.08 (.04)	.08	.04	.017
δr_{ts}	.73	.43 (.28)	.36 (.23)	.36	.20	.11
$\delta \Omega_b h^2 / \Omega_b h^2$.28	.12	.11	.06	.016	.008
$\delta \Omega_{nr} h^2 / h_0^2$.32	.14	.13	.08	.042	.02
$\delta \Omega_{vac} h^2 / h_0^2$.74	.36 (.23)	.33 (.21)	.26	.15	.06
$\delta \Omega_{m\nu} (h)^2 / h_0^2$.43	.38 (.30)	.29 (.25)	.26	.085	.03
τ_C	.33	.28	.25	.25	.20	.15
$\delta h/h$.23	.17	.11	.10	.05	.02
$\delta \sigma_8 / \sigma_8$.29	.86	.28	.60	.25	.14 [.05]
$\delta \mathcal{P}_\Phi^{1/2}(k_n) / \mathcal{P}_\Phi^{1/2}(k_n)$.24	.27	.19	.24	.19	.13 [.06]